Transp Porous Med (2013) 99:207–227
DOI 10.1007/s11242-013-0181-7

Linear Instability of a Horizontal Thermal Boundary Layer Formed by Vertical Throughflow in a Porous Medium: The Effect of Local Thermal Nonequilibrium

P. M. Patil · D. Andrew S. Rees

Received: 28 March 2013 / Accepted: 14 May 2013 / Published online: 31 May 2013

Abstract In this paper we investigate the onset of convection in a saturated porous medium where uniform suction into a horizontal and uniformly hot bounding surface induces a stationary thermal boundary layer. Particular attention is paid to how the well-known linear stability characteristics of this boundary layer are modified by the presence of local thermal nonequilibrium effects. The basic conduction state is determined and it is found that the boundary layer forms two distinct regions when the porosity is small or when the conductivity of the fluid is small compared with that of the solid. A linearised stability analysis is performed which results in an ordinary differential eigenvalue problem for the critical Darcy–Rayleigh number as a function of the wave number and the two nondimensional parameters, H and γ, which are associated with local thermal nonequilibrium. This eigenvalue problem is solved numerically by first approximating the equations by fourth order compact finite differences, and then the critical Rayleigh number is computed iteratively using the inverse power method and minimised over the wavenumber. The variation of the critical Rayleigh number and wavenumber with H and γ is presented. One of the unusual effects of local thermal nonequilibrium is that there exists a parameter regime within which the neutral curve is bimodal.

Keywords Porous medium · Surface suction · Local thermal nonequilibrium · Thermoconvective instability · Linear theory

P. M. Patil
Department of Mathematics, JSS's Banashankari Arts, Commerce and Shanti Kumar Gubbi Science College, Vidyagiri, Dharwad 580 004, India

P. M. Patil · D. A. S. Rees (✉)
Department of Mechanical Engineering, University of Bath, Bath BA2 7AY, UK
e-mail: D.A.S.Rees@bath.ac.uk

List of Symbols

c	Specific heat
c.c.	Complex conjugate
C_1, C_2	Constants defined in Eq. (25)
g	Gravity
h	Interfacial heat transfer coefficent
H	Nondimensional form of h
k	Disturbance wavenumber
k_f	Thermal conductivity of the fluid
k_s	Thermal conductivity of the solid
L	Vertical length scale
LTE	Local Thermal Equilibrium
LTNE	Local Thermal nonEquilibrium
K	Permeability
p	Pressure
Ra	Darcy–Rayleigh number
R_1, R_2	constants defined in Eq. (26)
t	Time
T	Dimensional temperature
u	Horizontal velocity
v	Vertical velocity
V_w	Magnitude of suction velocity
x	Horizontal coordinate
y	Vertical coordinate

Greek symbols

α	Diffusivity ratio
β	Thermal expansion coefficient
γ	Scaled conductivity ratio
ϵ	Porosity
θ	Fluid temperature
Θ	Disturbance fluid temperature
λ	Exponential growth rate
μ	Dynamic viscosity
Ξ	Generic variable
ρ	Density
σ	Spatial exponential growth rate
ϕ	Solid temperature
Φ	Disturbance solid temperature
ψ	Streamfunction
Ψ	Disturbance streamfunction

Subscripts and superscripts

b	Basic conducting state
f	Fluid phase
pm	Porous medium

s	Solid phase
w	Conditions at the wall
∞	Ambient conditions
$'$	Derivative with respect to y
$\hat{}$	Dimensional
$\tilde{}$	Scaled values

1 Introduction

In this paper we consider the onset of convection in a semi-infinite porous region which is bounded below by a uniformly hot permeable surface. The bounding surface is a suction surface through which fluid is drawn uniformly both spatially and in time. Thus, a thermal boundary layer is formed where the temperature field decays exponentially into the relatively cold region above. A similar boundary layer may be formed when saline water occupies a saturated region and evaporation at the upper surface causes an accumulation of solute at the upper surface. Both of these situations are potentially convectively unstable since fluid of higher density lies above fluid of lower density.

This generic problem of Darcy–Bénard type, which has been termed the Wooding problem after the pioneering paper of Wooding (1960), has been studied quite extensively by many authors with regard to both the linear and nonlinear stability properties of the boundary layer; see, for example, Sutton (1970), Homsy and Sherwood (1976), Riahi (1989), Wooding et al. (1997a), Wooding et al. (1997b), Duijn et al. (2002), Johannsen et al. (2006), and Pieters and Schuttelaars (2008), where some of these papers deal with solutal convection. Some authors have considered other features such as alternative boundary conditions (Jones and Persichetti 1986), non-Darcy effects (Shivakumara 1999), anisotropy (Rees and Storesletten 2002), non-Newtonian fluids (Shivakumara and Sureshkumar 2007), heterogeneity (Kuznetsov and Nield 2011), inclined temperature gradients (Nield 1998; Brevdo 2009), and a second diffusing component (Shivakumara and Khalili 2001). Further papers and discussion may be found in Rees (2009a,b).

In the present paper the focus of the research is on how the presence of local thermal nonequilibrium affects the well-known linear stability properties of the Wooding problem. In brief, local thermal nonequilibrium arises when the respective local mean values of the temperature of the fluid and the solid phases are not equal to one another. This often arises when rapid changes to the flow and temperature fields take place, such as when hot fluid is suddenly injected into a cold and relatively poorly conducting solid porous matrix. It may also arise in steady flows (see Rees 2003). In practice two heat transport equations are required, one for each phase, and each with a source/sink term which is proportional to the local temperature difference between the phases. Although the first paper to appear which deals with thermoconvective instability in porous media is the pioneering nonlinear analysis by Combarnous and Bories (1974), the first which considers the onset of convection is the one by Banu and Rees (2002), in which is presented a comprehensive numerical and asymptotic account of the onset criterion as a function of the governing parameters.

The effect of local thermal nonequilibrium on the Wooding problem turns out to be anything but a simple quantitative change. Rather, we find that the presence of poor heat transfer between the phases leads to a natural stratification of the basic thermal boundary layer. This, in turn, generates bimodal neutral curves in part of the parameter space. We employ fourth-order compact finite difference methods in conjunction with the inverse power method to determine the onset criterion for convection. Comprehensive details of the variation of the onset criterion are presented.

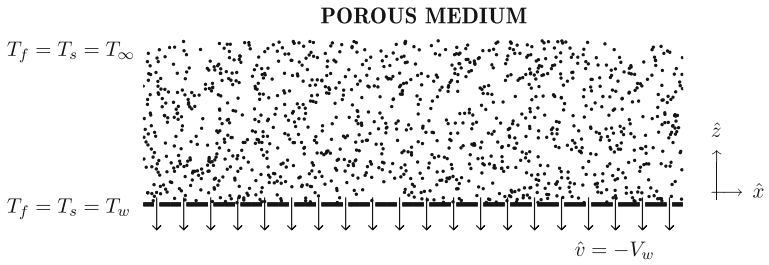

Fig. 1 Definition sketch of the configuration being studied

2 Governing Equations

A saturated porous medium is bounded from below by a uniformly hot horizontal surface through which fluid is drawn at the uniform velocity, $-V_w$. The surface is maintained at the temperature, T_w, while the ambient temperature is T_∞, where $T_w > T_\infty$. The porous medium itself is homogeneous and isotropic, and both Darcy's law and the Boussinesq approximation are assumed to hold. The solid and fluid phases are assumed not to be in local thermal equilibrium, i.e. local thermal nonequilibrium conditions prevail. The co-ordinate system and flow configuration are as shown in Fig. 1.

The governing equations for the evolution of the flow and temperature fields of both the fluid and solid phases of a rigid porous medium have been described by Nield and Bejan (2006) and are given by,

$$\frac{\partial \hat{u}}{\partial \hat{x}} + \frac{\partial \hat{w}}{\partial \hat{z}} = 0, \tag{1}$$

$$\hat{u} = -\frac{K}{\mu}\frac{\partial \hat{p}}{\partial \hat{x}}, \tag{2}$$

$$\hat{w} = -\frac{K}{\mu}\left(\frac{\partial \hat{p}}{\partial \hat{z}} - \rho_f g\beta(T_f - T_\infty)\right), \tag{3}$$

$$\epsilon(\rho c)_f \frac{\partial T_f}{\partial \hat{t}} + (\rho c)_f\left(\hat{u}\frac{\partial T_f}{\partial \hat{x}} + \hat{w}\frac{\partial T_f}{\partial \hat{z}}\right) = \epsilon k_f \nabla^2 T_f + h(T_s - T_f), \tag{4}$$

$$(1-\epsilon)(\rho c)_s \frac{\partial T_s}{\partial \hat{t}} = (1-\epsilon)k_s \nabla^2 T_s - h(T_s - T_f). \tag{5}$$

In these equations $\hat{x}$ and $\hat{z}$ are the horizontal and vertical coordinates, respectively, while $\hat{u}$ and $\hat{w}$ are the corresponding velocities. In addition $\hat{t}$ is time, $\hat{p}$ is the pressure, T the temperature, K the permeability, μ the dynamic viscosity, g gravity, β the coefficient of cubical expansion, ϵ the porosity, ρ the density, c the specific heat, k the conductivity, and h the interfacial heat transfer coefficient. The subscripts, f and s, denote fluid and solid, respectively, while ∞ denotes the ambient state far from the heated surface. The boundary conditions are that,

$$\hat{w} = -V_w, \quad T_f = T_s = T_w \quad \text{on} \quad \hat{z} = 0, \tag{6}$$

and

$$\hat{u} \longrightarrow 0, \quad T_f, T_s \longrightarrow T_\infty \quad \text{as} \quad \hat{z} \to \infty, \tag{7}$$

where the constant value $V_w > 0$ corresponds to suction.

The presence of two temperature fields, one for the solid porous matrix and one for the saturating fluid, means that it is possible for the phases to have different temperatures at the same point in space. This is true in the macroscopic sense of the phases having different mean temperatures, where T_s and T_f are defined by their respective averages over a small Representative Elementary Volume. On the microscopic level there remains a continuity of temperature and heat flux at the interface between the phases.

The inter-phase heat transfer coefficient, h, which is used to model the microscopic transfer of heat between the phases, is worthy of special interest. Small values of h generally imply that such heat transfer takes place slowly and in the presence of a flow it remains possible for T_s and T_f to have different profiles even in the steady state. This situation is known as Local Thermal Nonequilibrium (LTNE), as opposed to Local Thermal Equilibrium (LTE), which occurs when h is sufficiently large and for which a single heat transport equation is used.

In general, h will be a function of the geometry of the porous medium, the local flow and the conductivities of the phases. There are many works which cite correlations for h, such as that of Wakao and Kaguei (1982) (see the review by Rees and Pop 2005), but recent papers by Rees (2009a; 2009b, 2010) draw attention to the fact that such correlations do not satisfy essential mathematical symmetries in the limit of zero flow. Some analytical expressions for h were derived in Rees (2010) and numerical results presented for structured and random media in both two (Rees 2010) and three dimensions (Rees 2009a; 2009b). For the present problem, these correlations will not apply because of the present of a flow, but h will nevertheless be uniform spatially given that the present analysis is a linear stability theory and that the imposed background flow is uniform and steady.

The present problem does not possess a natural length scale although the velocity scale, V_w, may be used to define a length scale, L, in terms of V_w and the other natural properties of the porous medium in the following way: $L = k_{pm}/V_w(\rho c)_f$. Nondimensional variables may now be introduced by means of the scalings,

$$(\hat{x}, \hat{z}) = L(x, z), \qquad (\hat{u}, \hat{w}) = V_w(u, w),$$

$$(T_f, T_s) = T_\infty + (T_w - T_\infty)(\theta, \phi), \qquad \hat{t} = \frac{L^2(\rho c)_{pm}}{k_{pm}} t, \tag{8}$$

where all quantities, denoted generically by Ξ, which are associated with the porous medium have been defined according to the weighted arithmetic mean

$$\Xi_{pm} = \epsilon\, \Xi_f + (1 - \epsilon)\, \Xi_s. \tag{9}$$

For two-dimensional flow we may define the streamfunction, ψ, according to $u = -\psi_z$ and $w = \psi_x$ and Eqs. (1–5) now take the nondimensional form,

$$\frac{\partial^2 \psi}{\partial x^2} + \frac{\partial^2 \psi}{\partial z^2} = Ra\, \frac{\partial \theta}{\partial x}, \tag{10}$$

$$\left(\frac{\gamma + 1}{\gamma + \alpha}\right)\frac{\partial \theta}{\partial t} + \left(\frac{\gamma + 1}{\gamma}\right)\left(\frac{\partial \psi}{\partial x}\frac{\partial \theta}{\partial z} - \frac{\partial \psi}{\partial z}\frac{\partial \theta}{\partial x}\right) = \frac{\partial^2 \theta}{\partial x^2} + \frac{\partial^2 \theta}{\partial z^2} + H(\phi - \theta), \tag{11}$$

$$\alpha\left(\frac{\gamma + 1}{\gamma + \alpha}\right)\frac{\partial \phi}{\partial t} = \frac{\partial^2 \phi}{\partial x^2} + \frac{\partial^2 \phi}{\partial z^2} + \gamma H(\theta - \phi). \tag{12}$$

The four nondimensional parameters, H, γ, α and Ra, are, respectively, the inter-phase heat transfer coefficient, the porosity-modified conductivity ratio, the diffusivity ratio and the

Darcy–Rayleigh number based on the properties of the porous medium; they are given by

$$H = \frac{hL^2}{\epsilon k_f}, \qquad \gamma = \frac{\epsilon k_f}{(1-\epsilon)k_s},$$

$$\alpha = \frac{(\rho c)_s}{(\rho c)_f}\frac{k_f}{k_s}, \qquad Ra = \frac{\rho_f g\beta(T_w - T_\infty)KL}{\mu\kappa_{\rm pm}}. \tag{13}$$

In view of Eq. (8), the boundary conditions for Eqs. (10)–(12) are that $\psi = -x$ and $\theta = \phi = 1$ at $z = 0$, and that $\psi_z, \theta, \phi \to 0$ as $z \to \infty$.

We note that the complicated coefficients in Eqs. (11) and (12) have distinctive meanings in terms of ratios of conductivities and diffusivities since

$$\frac{\gamma+1}{\gamma+\alpha} = \frac{\alpha_{pm}}{\alpha_f}, \qquad \frac{\gamma+1}{\gamma} = \frac{k_{pm}}{\epsilon k_f} \qquad \text{and} \qquad \alpha\Big(\frac{\gamma+1}{\gamma+\alpha}\Big) = \frac{\alpha_{pm}}{\alpha_s}. \tag{14}$$

We also note that when LTE conditions prevail, i.e. when $H \gg 1$, then $\theta \sim \phi$, and the source/sink terms on the right hand sides of (11) and (12) may be eliminated to yield,

$$\frac{\partial\theta}{\partial t} + \frac{\partial\psi}{\partial x}\frac{\partial\theta}{\partial z} - \frac{\partial\psi}{\partial z}\frac{\partial\theta}{\partial x} = \frac{\partial^2\theta}{\partial x^2} + \frac{\partial^2\theta}{\partial z^2}. \tag{15}$$

3 Basic State

If we assume that the basic state for the temperature is steady and a function solely of z then Eqs. (11) and (12) reduce to the following form,

$$\theta'' + \Big(\frac{\gamma+1}{\gamma}\Big)\theta' + H(\phi - \theta) = 0, \tag{16}$$

$$\phi'' + H\gamma(\theta - \phi) = 0, \tag{17}$$

where the basic flowfield is given by $\psi = -x$ and where primes denote derivatives with respect to z. The boundary conditions are that

$$z = 0: \qquad \theta = \phi = 1, \tag{18}$$

and

$$z \to \infty: \qquad \theta, \phi \to 0. \tag{19}$$

Before solving Eqs. (16)–(19) it is important to note that, while fluid velocities in porous media are usually mean values over the whole porous medium (i.e. the superficial velocity), the presence of LTNE often allows the magnitude of the intrinsic velocity (i.e. the mean value over the fluid phase only) to be felt instead. In the present case, the coefficient of θ' in Eq. (16) may be taken to represent an effective fluid suction velocity. Thus when either H or γ is large, the leading order form of the solution to Eqs. (16)–(19) takes the LTE form,

$$\theta \sim e^{-z}, \quad \phi \sim e^{-z}, \tag{20}$$

and therefore suction velocity which determines the thickness of the thermal boundary layer is the superficial velocity, i.e. $w = -1$ in nondimensional terms. On the other hand, when H is small, the thermal fields of the fluid and solid phases are almost decoupled, and the leading order forms of the basic solution become,

$$\theta \sim e^{-(\gamma+1)z/\gamma}, \quad \phi \sim e^{-\sqrt{H\gamma}z}. \tag{21}$$

The thickness of the boundary layer in the fluid phase is proportial to $\gamma/(\gamma+1)$, which is the intrinsic suction velocity, while the solid phase has a very thick thermal boundary layer due to the very small amount of heat being lost to the fluid phase. Even for moderate values of H we may also predict that there will be a thin thermal boundary layer of thickness $O(\gamma)$ in the fluid phase when $\gamma \ll 1$ and thick outer layer which exists primarily in the solid phase.

Equations (16) and (17) admit four linearly independent solutions of the form, $e^{\sigma z}$, which satisfy the equation,

$$\sigma\left[\sigma^3 + \frac{\gamma+1}{\gamma}\sigma^2 - H(\gamma+1)\sigma - H(\gamma+1)\right] = 0. \tag{22}$$

Clearly one of the values of σ is zero and another is always positive, and therefore both have to be discarded because they correspond to terms which do not satisfy the far-field boundary conditions for θ and ϕ. The remaining two roots are always negative, since the sign of the coefficient of σ^2 in Eq. (22) is positive. The detailed solution of Eq. (22) may be obtained analytically by first employing Cardan's formula for the solution of a cubic equation, the details of which are straightforward and have been omitted. We may now write the solutions for θ and ϕ in the form,

$$\theta = C_1 e^{\sigma_1 z} + C_2 e^{\sigma_2 z}, \tag{23}$$

$$\phi = R_1 C_1 e^{\sigma_1 z} + R_2 C_2 e^{\sigma_2 z}, \tag{24}$$

where

$$C_1 = \frac{R_2 - 1}{R_2 - R_1}, \qquad C_2 = \frac{1 - R_1}{R_2 - R_1}, \tag{25}$$

$$R_j = 1 - \frac{1}{H}\left[\sigma_j^2 + \left(\frac{\gamma+1}{\gamma}\right)\sigma_j\right], \qquad j = 1, 2, \tag{26}$$

and where σ_1 and σ_2 are the two admissible (i.e. negative) roots of Eq. (22).

Some representative temperature profiles of both phases are given in Figs. 2 and 3 as functions of H and γ. Figure 2a and b correspond to $\gamma = 1$ and 0.1, respectively, while H takes values from 100 down to 0.1. The outer curves correspond to the lowest value of H. In Fig. 2a the value $H = 100$ corresponds to near-LTE conditions since there is very little difference between the temperature profiles of the two phases. When H decreases the thermal boundary layer thickness of the solid phase increases substantially because less heat is lost to the fluid phase thereby allowing it to conduct further away from the heated surface before the cumulative effect of heat transfer to the fluid eventually decreases the temperature to zero. On the other hand, when H decreases, the thickness of the fluid boundary layer decreases because its temperature field begins to be affected much more by the magnitude of the intrinsic velocity of the fluid, rather than by the superficial velocity which occurs when the phases are in LTE, as discussed above.

Figure 2a and b may also be compared directly. In contrast to the case in Fig. 2a, it is clear from Fig. 2b that $H = 100$ is not sufficiently large for the phases to be regarded as being in LTE because there is quite a large difference between the respective temperatures of the phases, particularly when z takes small to moderate values. While LTNE effects are generally stronger when γ takes smaller values, the temperature profile of the fluid phase now begins to show two distinct zones, an inner region which exhibits rapid decay and an outer region which has a much slower decay rate. The solid phase seems to display only the slow decay rate.

Figure 3a and b show temperature profiles for $H = 10$ and $H = 1$, respectively, for a selection of values of γ. Again the transition between LTE conditions (large values of γ)

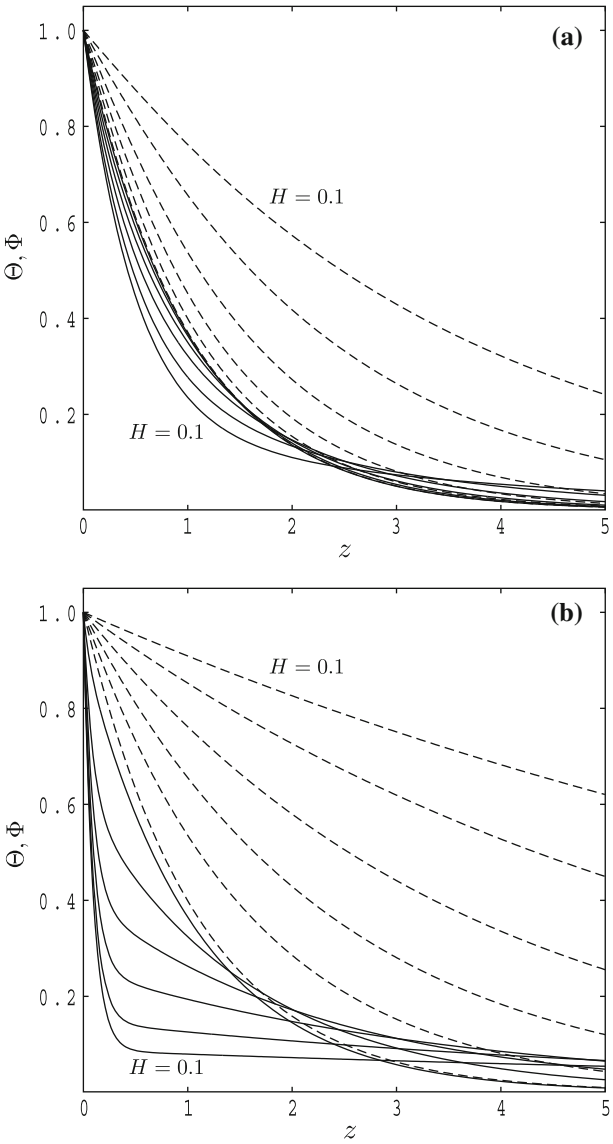

Fig. 2 Profiles of the temperature of the solid phase (*dashed lines*) and the fluid phase (*continuous lines*) for **a** $\gamma = 1$ and **b** $\gamma = 0.1$, and for H taking the values, $H = 100$, 10, 3, 1, 0.3 and 0.1

and strongly LTNE conditions (low values of γ) may be seen easily; in each case the two outermost curves correspond to the smallest value of γ. When γ decreases to values below $\gamma = 1$ the double-layer structure of the θ-profile mentioned above again becomes evident, as does the slow decay of the ϕ-profile. These figures also indicate that the inner layer becomes thinner as γ decreases while the outer layer becomes thicker, although the inner layer remains of roughly constant thickness as H decreases to small values. Quantitative information on this behaviour may be found by means of an asymptotic analysis of the solutions of Eq. (22)

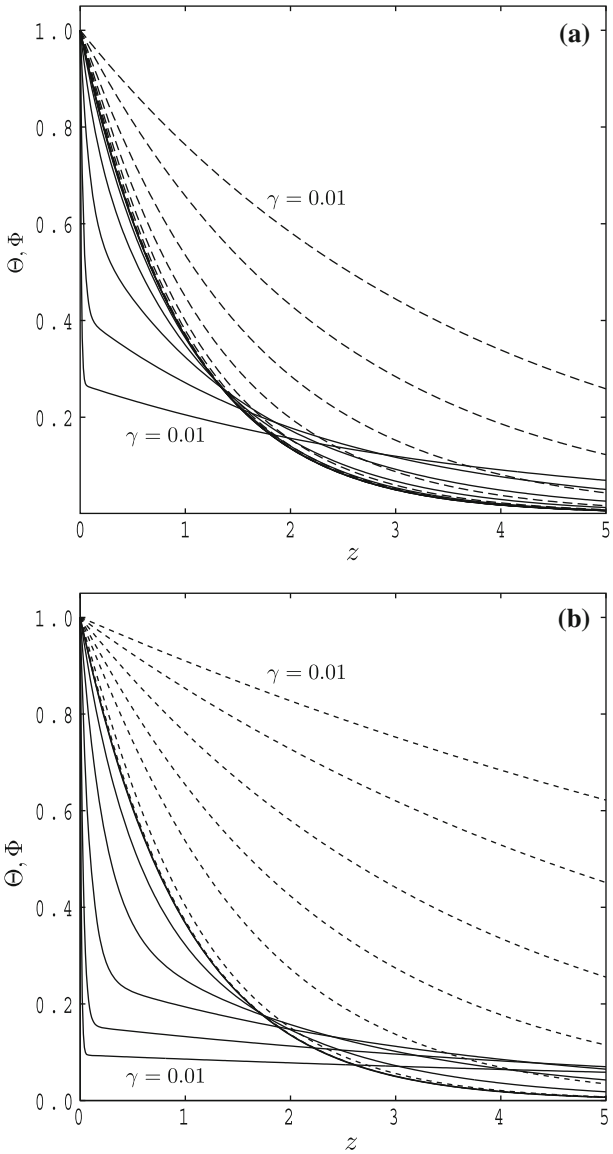

Fig. 3 Profiles of the temperature of the solid phase (*dashed lines*) and the fluid phase (*continuous lines*) for **a** $H = 10$ and **b** $H = 1$, and for γ taking the values, $\gamma = 100$, 10, 1, 0.3, 0.1, 0.03 and 0.01

in the limit as $\gamma \to 0$. Omitting the details of this analysis, which is straightforward but lengthy, we find that

$$\sigma_1 \sim -(H\gamma)^{1/2} - \frac{H\gamma}{2} - \frac{(H\gamma)^{3/2}}{8} - \frac{H\gamma^2}{8}, \tag{27}$$

$$\sigma_2 \sim \frac{1}{\gamma} - 1 - H\gamma + H\gamma^2. \tag{28}$$

Table 1 Values of σ_1 and σ_2 as functions of H and γ, together with the coefficients given in Eqs. (23)–(26)

H	γ	σ_1	σ_2	C_1	C_2	R_1C_1	R_2C_2
10	100	−0.999990	−31.785663	0.999990	0.000010	1.000991	−0.000991
10	30	−0.999892	−17.624496	0.999886	0.000114	1.003229	−0.003229
10	10	−0.999084	−10.543474	0.998988	0.001012	1.009061	−0.009061
10	3	−0.991600	−6.524453	0.990094	0.009906	1.023645	−0.023645
10	1	−0.952483	−5.135923	0.941665	0.058335	1.035619	−0.035619
10	0.3	−0.818763	−6.112242	0.790731	0.209269	1.018272	−0.018272
10	0.1	−0.628061	−11.849939	0.607245	0.392755	1.002817	−0.002817
10	0.03	−0.419783	−34.622239	0.412666	0.587334	1.000151	−0.000151
10	0.01	−0.270457	−101.098921	0.268523	0.731477	1.000060	−0.000060
1	100	−0.999900	−10.055430	0.999889	0.000111	1.009987	−0.009987
1	30	−0.998891	−5.588101	0.998650	0.001350	1.033007	−0.033007
1	10	−0.990214	−3.388319	0.986173	0.013827	1.093382	−0.093382
1	3	−0.912396	−2.314835	0.855403	0.144597	1.183930	−0.183930
1	1	−0.688892	−2.481194	0.569314	0.430686	1.083526	−0.083526
1	0.3	−0.434297	−4.556041	0.374691	0.625309	1.009170	−0.009170
1	0.1	−0.273033	−11.090243	0.254685	0.745315	1.000609	−0.000609
1	0.03	−0.159190	−34.362437	0.155286	0.844714	1.000070	−0.000070
1	0.01	−0.095162	−101.009907	0.094380	0.905620	1.000647	−0.000647
0.1	100	−0.998904	−3.185346	0.998403	0.001597	1.109067	−0.109067
0.1	30	−0.984823	−1.798618	0.966456	0.033544	1.428173	−0.428173
0.1	10	−0.831162	−1.292657	0.527082	0.472918	1.704835	−0.704835
0.1	3	−0.491537	−1.416353	0.221290	0.778710	1.136932	−0.136932
0.1	1	−0.288362	−2.049970	0.171872	0.828128	1.020186	−0.020186
0.1	0.3	−0.161634	−4.356325	0.129329	0.870671	1.001380	−0.001380
0.1	0.1	−0.095519	−11.009084	0.087606	0.912394	1.000104	−0.000104
0.1	0.03	−0.053332	−34.336247	0.051890	0.948110	1.000544	−0.000544
0.1	0.01	−0.031126	−101.000997	0.031051	0.968949	1.006907	−0.006907

Therefore, the inner layer has thickness of $O(\gamma)$ while the outer layer has thickness of $O(\gamma^{-1/2})$. These results are confirmed by the data given in Table 1, which also presents the value of the coefficients, C_1, C_2, R_1C_1 and R_2C_2 which appear in Eqs. (25) and (26) and which are the coefficients of the exponentials in the solutions for θ and ϕ.

A further comparison between Fig. 3a and b shows that the amplitude of the outer layer component of the fluid temperature field decreases with γ. Given that σ_2 has been taken to represent the inner layer in Eq. (28), this means that the amplitude C_1 in (25) decreases, and C_2 increases. Again, the detailed asymptotic analysis referred to above yields the following leading order information as $\gamma \to 0$:

$$C_1 \sim (H\gamma)^{1/2}, \qquad C_2 \sim 1 - (H\gamma)^{1/2}, \qquad R_1 \sim (H\gamma)^{-1/2}, \qquad R_2 = O(\gamma^3), \quad (29)$$

which confirm the numerical result. Therefore, the leading order temperature profiles become,

$$\theta \sim (H\gamma)^{1/2} e^{-(H\gamma)^{1/2} z} + [1 - (H\gamma)^{1/2}] e^{-z/\gamma}, \qquad \phi \sim e^{-z/\gamma}, \quad (30)$$

when $\gamma \ll 1$.

Finally, it is important to point out that, while one might expect neutral stability curves to be unimodal for the present problem, just as it is when the phases are in LTE, the shape of the basic fluid profiles hint that neutral curves might be bimodal in some circumstances. The reasoning for this lies in the observation that when γ is small, one may define local Darcy–Rayleigh numbers for both the inner and outer layers, ones which are based upon the respective total temperature drop and the height of those layers. In general one of these Darcy–Rayleigh numbers will be larger than the other, and convection is most likely to arise in the layer with the larger value. The critical wavelength of the cellular pattern will then be proportional to the thickness of the dominant layer. It is also conceivable that the values of Ra are comparable in some parameter regimes, and that two modes with different wavelengths will compete. We will see that bimodal curves do indeed arise for the present problem and may be traced directly to this natural thermal layering of the basic state.

4 Linear Stability Analysis

The linear stability analysis of the basic state given by Eqs. (23) and (24) and $\psi_b = -x$ may be investigated by setting as

$$(\psi, \theta, \phi) = (\psi_b, \theta_b, \phi_b) + \Big[\Big(i\Psi(z), \Theta(z), \Phi(z)\Big)e^{\lambda t + ikx} + \text{c.c.}\Big], \tag{31}$$

where the b-subscript denotes the basic state given above, k is the horizontal wavenumber, λ the exponential growth rate. and where c.c. denotes the complex conjugate. The substitution of Eq. (31) into the governing Eqs. (10)–(12) followed by linearization yields the following set of perturbation equations:

$$\Psi'' - k^2\Psi = Ra\, k\, \Theta, \tag{32}$$

$$\Theta'' + \Big(\frac{\gamma+1}{\gamma}\Big)\Theta' - k^2\Theta + H(\Phi - \Theta) + \Big(\frac{\gamma+1}{\gamma}\Big)k\Big[\sigma_1 C_1 e^{\sigma_1 z} + \sigma_2 C_2 e^{\sigma_2 z}\Big]\Psi = \lambda\Theta, \tag{33}$$

$$\Phi'' - k^2\Phi + H\gamma(\Theta - \Phi) = \alpha\lambda\Phi, \tag{34}$$

subject to the boundary conditions,

$$z = 0: \quad \Psi = \Theta = \Phi = 0, \qquad z \to \infty: \quad \Psi, \Theta, \Phi \to 0. \tag{35}$$

5 Numerical Procedure

Equations (32)–(35) may be interpreted as representing an eigenvalue problem for the exponential growth rate, λ, as a function of Ra, k, H, γ and α. The solutions for Ψ, Θ and Φ may be complex, but we will assume that the principle of exchange of stabilities applies and therefore solutions are real and that the onset of convection is stationary, i.e. that λ may be set to zero. Thus, Eqs. (32)–(35) now form an eigenvalue problem for Ra as a function of k and the remaining two LTNE parameters, H and γ.

Neutral curves may be obtained by solving Eqs. (32)– (35) numerically. We first discretize the spatial derivatives using a fourth-order compact finite difference scheme on a uniform grid, based upon the methodology described by Spotz (1995). The finite difference stencils are straightforward to derive, but quite lengthy to present and they are omitted here. In general, Eqs. (32)–(35) are solved on a grid of 100 uniform intervals in the range, $0 \le z \le 10$. We

claim at least four significant figures of accuracy in all cases presented here. For the reasons described above, an inner thermal layer exists when γ is small, and we therefore restrict our simulations to the range, $\gamma \geq 0.1$.

The resulting difference equations may be rearranged into a matrix/vector form, and we then apply a suitable version of the inverse Power method (see, for example, Jennings and McKeown 1992). This yields the smallest value of Ra for neutral stability for the chosen set of parameters. The speed of convergence of the inverse power method depends on the ratio of the two smallest eigenvalues, and it was found that convergence is relatively slow for large values of k where Ra is also relatively large but where neighbouring modal values of Ra are at an $O(1)$ separation. On the other hand, convergence is relatively fast for small wavenumbers because the modes remain widely separated in terms of Ra. The inverse power method was selected over and above a straightforward Runge–Kutta/shooting method scheme primarily because Eqs. (32)–(35) become stiff whenever k, H or γ is large; the need to consider the approach to LTE is essential, particularly because of the need to confirm that the well-known LTE solution is obtained in the large-H or large-γ limits.

The need to compute the critical Rayleigh number and the corresponding wavenumber means that some form of minimisation of Ra over k must be implemented. This was undertaken by embedding the inverse Power Method algorithm inside a straightforward Newton-Raphson iteration scheme to find where $dRa/dk = 0$.

6 Results and Discussion

Some representative neutral curves are displayed in Fig. 4 for a set of values of H where $\gamma = 1$ has been chosen and which corresponds to when the effective conductivities of the fluid and solid phases are equal, i.e. when $\epsilon k_f = (1-\epsilon)k_s$. The neutral curves display the classical shape which is associated with most Bénard-like problems in which there is a single minimum. When H takes large values we recover the LTE result in which $Ra_c = 14.3552$ and $k_c = 0.7589$ (Rees 2009a). When H decreases the critical Rayleigh number increases slightly but the critical wavenumber increases quite substantially.

Figure 5 shows the disturbance profiles corresponding to the minima in some of the neutral curves displayed in Fig. 4. In all cases the strength of the disturbance within the fluid phase is greater than that in the solid phase. Perhaps this is due to the fact that the buoyancy term forms part of the heat transport equation for the fluid, rather than the solid, and that the response of the solid phase is in part a reaction to what is happening to the fluid phase. That this is so is demonstrated by the decreasing amplitude of the ϕ-profile compared with the θ-profile as H decreases. We also note that the thickness of the θ-disturbance profile again decreases with H, just as the basic θ-profile does, and this is again due to the intrinsic suction velocity becoming the effective velocity in terms of its effects on the fluid temperature.

While Fig. 4 shows neutral curves with a single minimum, our earlier discussion of the possible role played the inner and outer layers, when they are distinct, in the formation of neutral curves with two minima, is demonstrated to be correct in Fig. 6. This figure displays neutral curves when $\gamma = 0.18$ with H taking discrete values between 1 and 2. The lowest curve (i.e. the one with $k_c \simeq 1.5$) corresponds to $H = 2$ and the critical wavenumber is relatively low; this corresponds to an onset mode profile which is located mainly in the outer region of the basic state. As H decreases from 2 a second minimum at a higher wavenumber appears and, when $H \simeq 1.7284$, the two minima then correspond to the same critical Rayleigh number. At still lower values of H the second minimum takes over as the dominant one, given

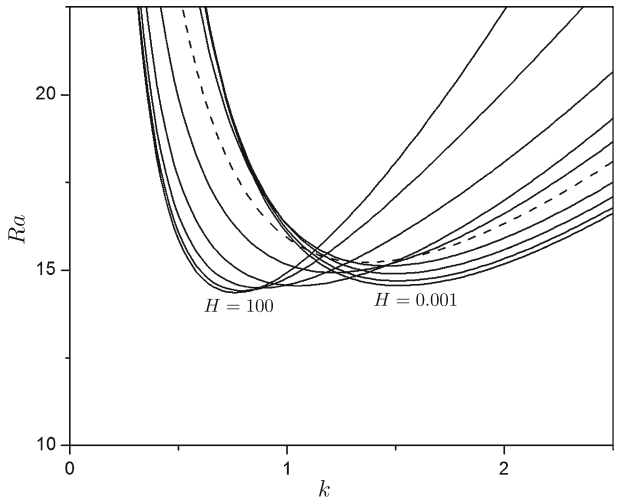

Fig. 4 Some neutral curves for $\gamma = 1$ and $H = 0.001$, 0.003, 0.01, 0.03, 0.1, 0.3, 1, 3, 10 and 100. The *dashed line* corresponds to $H = 0.1$

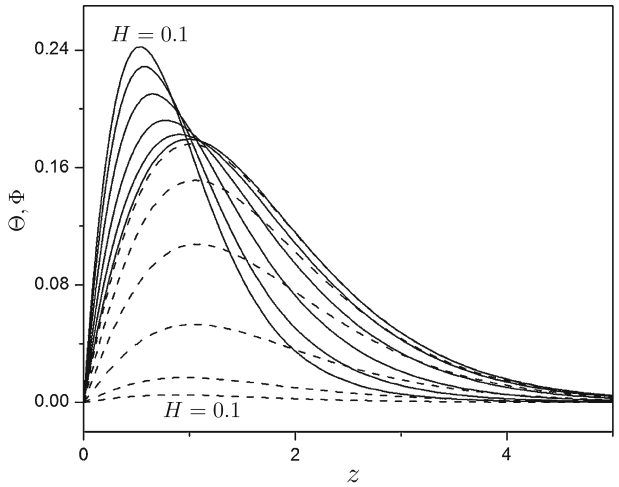

Fig. 5 Disturbance profiles corresponding to $\gamma = 1$ with $H = 0.1$, 0.3, 1, 3, 10 and 100. The *continuous lines* represent the fluid temperature profiles and the *dashed lines* the solid temperature profiles

that it now corresponds to the smaller critical value of Ra. This onset mode has temperature profiles which are concentrated in the inner region of the basic state.

This sudden transition from a mode with a relatively small wavenumber to one with a relatively large one is important at least in terms of understanding fully the onset properties of the title problem. We summarise the transition in Figs. 7, 8, 9 and 10. Figure 7 shows a selection of neutral curves in the range $0.14 \leq \gamma \leq 0.2$ which have double minima, i.e. where both minima in any chosen neutral curve correspond to the same Rayleigh number. The detailed data for these double minima are given in Table 2. The minimum value of γ in this range corresponds to the value beyond which we cannot guarantee the accuracy of the basic profiles because of the decreasing thickness of the inner layer as γ decreases. The maximum

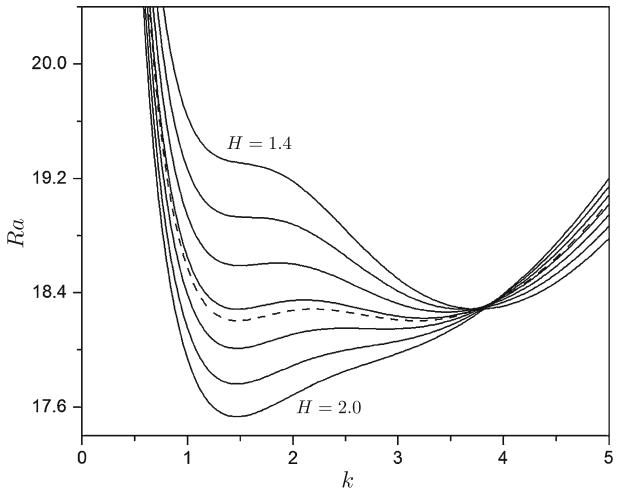

Fig. 6 Some neutral curves for $\gamma = 0.18$ showing the transition from a low critical wavenumber to a high critical wavenumber via a double minimum. The values of H are 1.4, 1.5, 1.6, 1.7, 1.8, 1.9 and 2.0. The *dashed line* corresponds to $H = 1.7284$ for which there is a double minimum

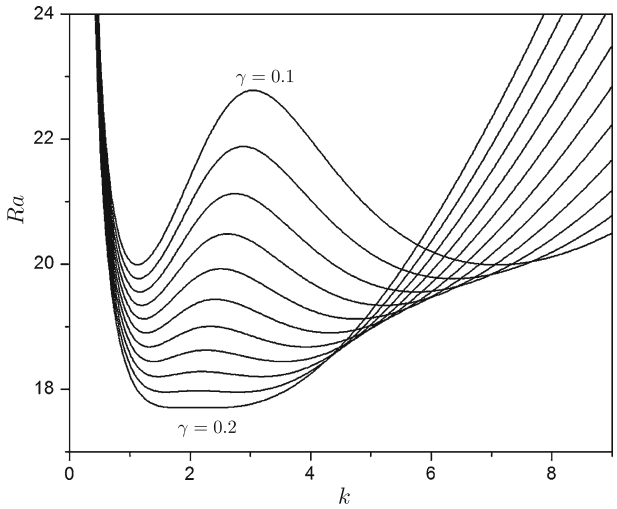

Fig. 7 Some neutral curves displaying double minima for $\gamma = 0.1(0.01)0.2$

value corresponds almost exactly to when the two minima have merged to form a neutral curve with a single quartic minimum. The quartic minimum actually arises when $\gamma \simeq 0.2015$ and $H = 1.6515$ and therefore we may state that neutral curves are always unimodal when $\gamma > 0.2015$. Bimodal curves of this kind have appeared elsewhere for Bénard-like problems; see Proctor and Jones (1988) who considered convection in superposed fluid layers and Rees and Riley (1990) who undertook an analysis of a porous layer with either two or three sublayers. However, these papers concern situations where the layering is mechanical whereas the present analysis is for a situation where a thermal layering arises naturally due to poor heat transfer between the fluid and solid phases.

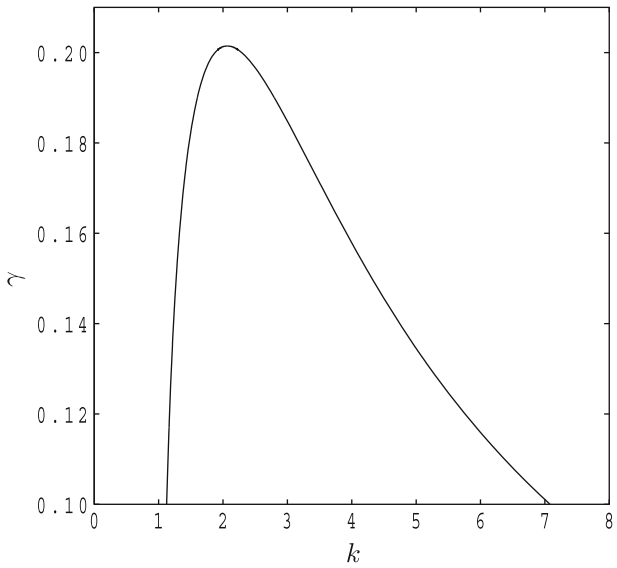

Fig. 8 Values of k_c at the double minimum points as γ varies

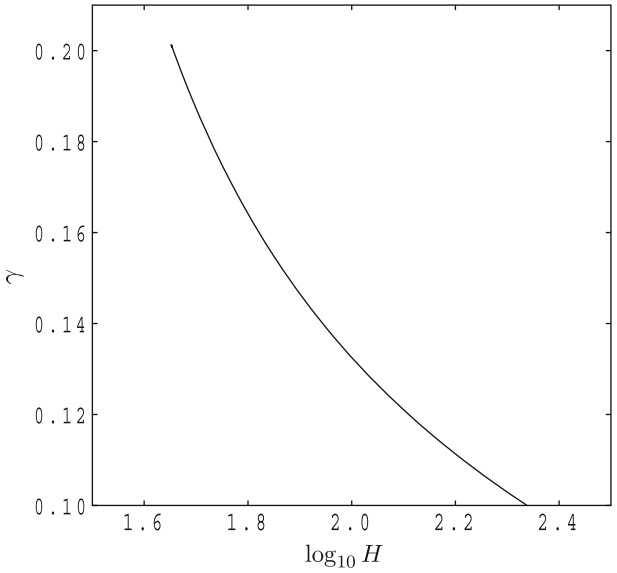

Fig. 9 Locus of double minimum points in (H, γ)–space

Figure 8 shows how the two values of the critical wavenumber vary with γ. We see clearly the merging of the two minima when γ is slightly greater than 0.2, and the increasing separation of the values as γ decreases. The curve as shown in this Figure has a parabolic maximum, and it is this nature which allowed us to calculate the location in (H, γ)-space of the quartic minimum in the neutral curve using a simple curve-fitting technique. The locus in (H, γ)-space where the neutral curve has a double minimum is shown in Fig. 9.

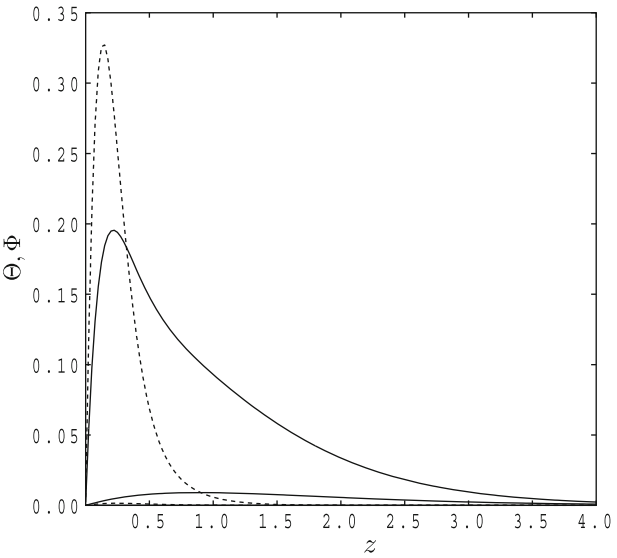

Fig. 10 Disturbance profiles for the case $\gamma = 0.14$, $H = 1.9441$ which has a double minimum. The critical wavenumbers are $k_{1c} = 1.2321$ (*continuous lines*) and $k_{2c} = 4.7458$ (*dashed lines*) and the common critical Rayleigh number is $Ra_c = 19.1275$. For each wavenumber the *upper curve* corresponds to the fluid temperature profile and the *lower* to that of the solid

Table 2 Values of H, Ra_c and the two critical wavenumbers for which the neutral curve has a double minimum as a function of γ

γ	H	$\log_{10} H$	Ra_c	$k_{c,1}$	$k_{c,2}$
0.2015	1.6515	0.2179	17.6670	2.0684	2.0684
0.2000	1.6562	0.2191	17.7042	1.8756	2.2899
0.1800	1.7284	0.2376	18.2044	1.4737	3.1788
0.1600	1.8214	0.2600	18.6786	1.3236	3.9182
0.1400	1.9441	0.2887	19.1275	1.2321	4.7458
0.1200	2.1101	0.3243	19.5574	1.1702	5.7597
0.1000	2.3382	0.3689	19.9918	1.1255	7.0797

A sample set of temperature profiles at the onset of convection for a double minimum case is shown in Fig. 10. Here, we have taken $\gamma = 0.14$ and the double minimum corresponds to $H = 1.9441$, $Ra = 19.1275$, $k_{c,\text{lower}} = 1.2321$ and $k_{c,\text{higher}} = 4.7458$. The continuous curves correspond to the lower value of k_c and both the fluid and solid temperature profiles are thick compared with the corresponding profiles for the higher value of k_c. In both cases the disturbance is much stronger in the fluid phase than in the solid phase.

Having explored in detail the various facets of the double minimum we are now in a position present comprehensive information on the critical values of the Rayleigh and wave numbers as functions of H and γ. The global behaviour of Ra_c and k_c is shown in Fig. 11 for chosen values of γ while H varies between 10^{-3} and 10^3. When H takes sufficiently large values Fig. 11a shows clearly that, for a fixed value of γ, the critical Rayleigh value decreases towards the well-known value of 14.3552 (see Rees 2009a, who adopted a LTE model) as H increases. It is also clear that this happens as γ increases for a fixed value of H. Both the $H \to \infty$ and $\gamma \to \infty$ limits correspond to Local Thermal Equilibrium, and therefore such behaviour is to be expected.

More surprising is that the same value of Ra_c is also attained in the limit as $H \to 0$, which is when strong local thermal nonequilibrium effects arise. That this is surprising is due to the universal experience of those authors who have studied the onset of convection in porous-Bénard problems where the critical Rayleigh number obeys a relationship of the following form,

$$\lim_{H\to 0} Ra_c = \frac{\gamma}{1+\gamma} \lim_{H\to\infty} Ra_c, \tag{36}$$

even though such a relationship has not been stated explicitly in such papers (see, for example, Banu and Rees 2002 and the many subsequent papers citing it). The property which is shared by these papers is that the thermal field remains of constant vertical thickness as H and/or γ vary. But when γ or H is small, the advective movement of heat is caused by the intrinsic fluid velocity, not the superficial velocity, and therefore the resistance to flow is less, which in turn reduces the critical Rayleigh number from that when γ or H is large. In the present work, the thermal boundary layer splits into two once again as $H \to 0$ and most of the temperature drop from the ambient to the surface value takes place within the inner layer. The effective lengthscale of the region within which convection occurs is now reduced from that when γ or H is large, and the reduction in the size of this region effectively cancels out the intrinsic velocity mechanism for early onset.

This physical argument may be put on a more precise mathematical foundation by formally setting H to be zero in Eqs. (32)–(34) and assuming that the exponential growth rate, λ, is zero. The disturbance equation for the solid phase is now irrelevant unless one wishes to undertake at least a two-term asymptotic analysis as $H \to 0$. The equations for the streamfunction and the fluid temperature now become,

$$\Psi'' - k^2\Psi = Ra\, k\Theta, \tag{37}$$

$$\Theta'' - k^2\Theta + \left(\frac{\gamma+1}{\gamma}\right)\Theta' + k\left(\frac{\gamma+1}{\gamma}\right)^2 e^{-(\gamma+1)z/\gamma}\Psi = 0. \tag{38}$$

If we now introduce the following scalings,

$$z = \frac{\gamma}{\gamma+1}\tilde{z}, \qquad k = \frac{\gamma+1}{\gamma}\tilde{k}, \qquad \Psi = \frac{\gamma}{\gamma+1}\tilde{\Psi}, \qquad \Theta = \tilde{\Theta}, \tag{39}$$

then Eqs. (37) and (38) become,

$$\frac{d^2\tilde{\Psi}}{d\tilde{z}^2} - \tilde{k}^2\tilde{\Psi} = Ra\,\tilde{k}\tilde{\Theta}, \tag{40}$$

$$\frac{d^2\tilde{\Theta}}{d\tilde{z}^2} + \frac{d\tilde{\Theta}}{d\tilde{z}} - \tilde{k}^2\tilde{\Theta} + \tilde{k}e^{-\tilde{z}}\tilde{\Psi} = 0. \tag{41}$$

On the other hand the large-H limit of Eqs. (32)–(34) corresponds to $\Theta = \Phi$ at leading order, and if we again set $\lambda = 0$, then multiply all terms in Eq. (33) by γ and add each side of that equation to the corresponding sides of Eq. (34), then we obtain a system which is identical to Eqs. (37) and (38) upon removing the tildes. Therefore the stability properties of the limiting cases, $H \to 0$ and $H \to \infty$, are identical with regard to the Rayleigh number. However, the sole difference between these limits is brought about by the scalings in Eq. (39). These mean that the critical wavenumber in the $H \to 0$ limit is greater by a factor of $(\gamma+1)/\gamma$ than those in the $H \to \infty$ limit. This is borne out by brief glance at the small-H behaviour of the wavenumber curves shown in Fig. 11b.

At moderate values of H in Figs. 11a and b we encounter the region where double minima occur when γ is sufficiently small. In Fig. 11a, the bullet symbol marks where the quartic

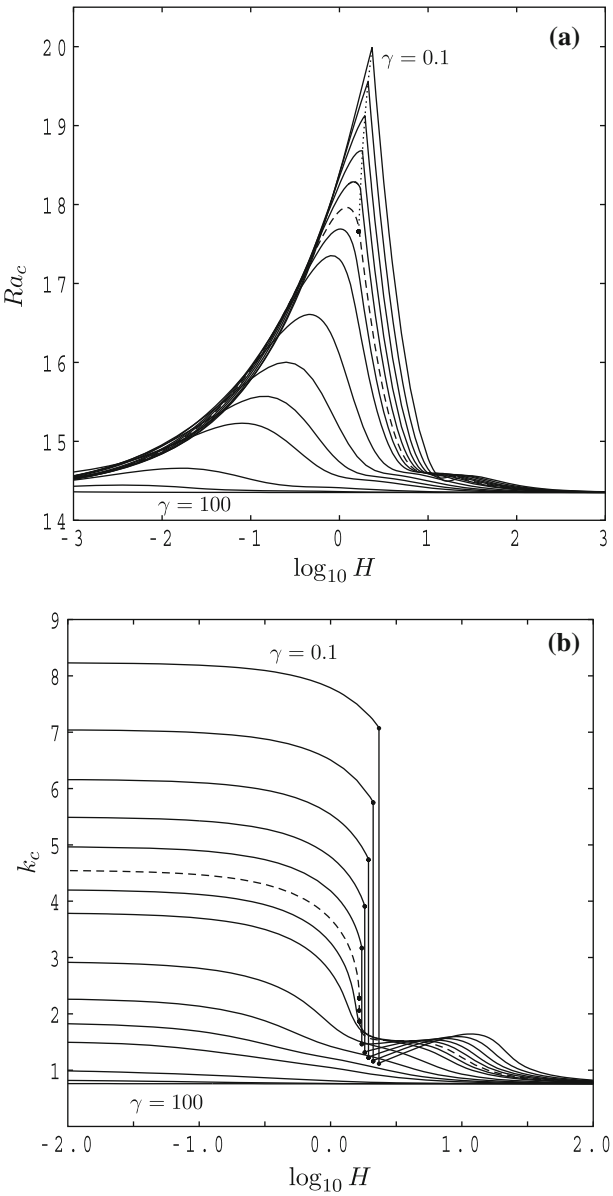

Fig. 11 Variation of **a** Ra_c and **b** k_c with $\log_{10} H$ for the following values of γ: 0.1, 0.12, 0.14, 0.16, 0.18, 0.2, 0.22, 0.25, 0.35, 0.5, 0.7, 1, 3, 10 and 100. In **a** the *dashed line* corresponds to the locus of double minima while the *bullet* is the quartic point. In **b** the *bullet points* correspond to where the critical wavenumber changes discontinuously and the *dashed line* to the case, $\gamma = 0.2$

minimum is and the locus of double minima is given by the dotted line. In Fig. 11b, which shows the critical wavenumber variation with $\log_{10} H$ for chosen values of γ, the bullet symbols denote where the critical wavenumber changes discontinuously as a double minimum is passed. The dotted curve in both Figures corresponds to $\gamma = 0.2$. The detailed behaviours of

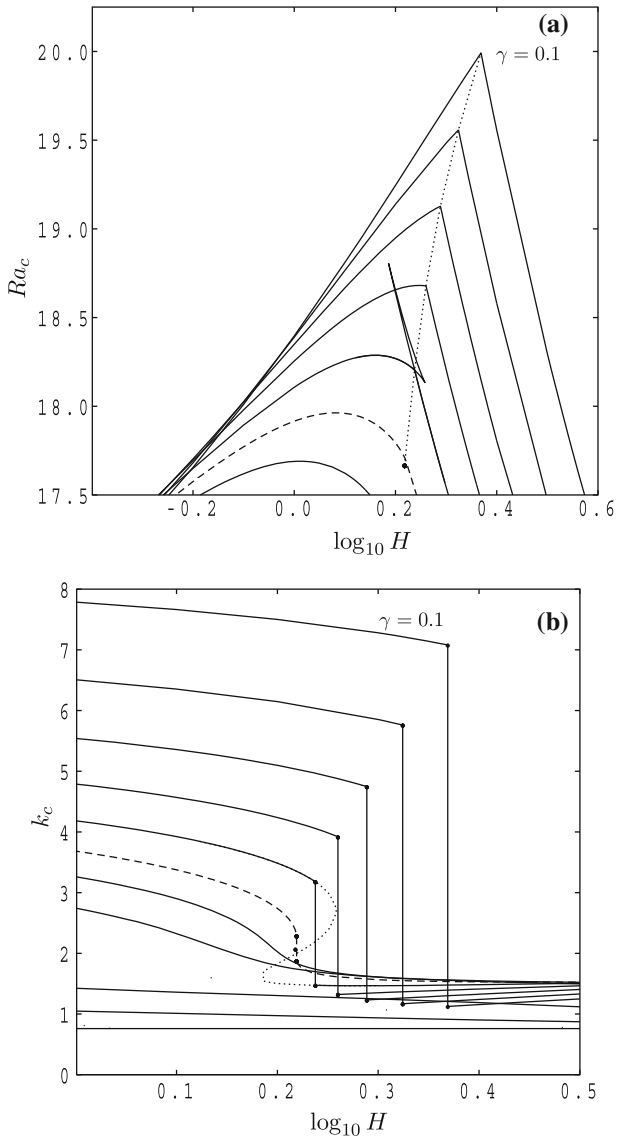

Fig. 12 Close-up views of the central sections of the curves shown in Fig. 11

these curves near the double minimum locus are difficult to see and therefore we show that detail in Fig. 12a and b.

Figure 12a shows that part of Fig. 11a which lies close to the locus of double minima, and which is again given by the dotted line. The discontinuity of the slope of the different curves as they pass through the double minimum locus is evident. For the case $\gamma = 0.18$ we show explicitly the variation with $\log_{10} H$ of both the minima and the intermediate maximum of the neutral curve, and we may therefore see the range of $\log_{10} H$ over which the neutral curve has two minima. This 'loop', which is terminated by two cusps, becomes larger as

γ decreases, and disappears altogether when γ increases towards the quartic point value of 0.2015 quoted above.

The corresponding variation in the wavenumber is shown in Fig. 12b. The jump in the critical wavenumber is shown explicitly. Again, for the case $\gamma = 0.18$, we have shown the complete variation in the wavenumber which accounts for both minima and the maximum in the neutral curve; this is the dotted curve. The extra S-shaped part of the curve, which corresponds to the maximum and the inferior minimum in the neutral curve, grows substantially as γ decreases, but shrinks and disappears altogether as $\gamma \to 0.2015$. In both Fig. 12a and 12b the $\gamma = 0.2$ case is shown as a dashed line for ease of reference.

7 Conclusions and Further Comments

In this paper we have considered the effects of local thermal nonequilibrium on the linear stability of the thermal boundary which forms above a hot surface with constant downward throughflow. In the first instance we found that the basic temperature field is altered from the pure exponential form which arises when the phases are in LTE. Small values of either γ or H cause the boundary layer to split into two distinct regions, an inner one, which arises because of the effect of the intrinsic suction velocity, and an outer one, which is due to the poor transfer of heat between the phases. This natural thermal layering has, as its consequence, the generation of neutral curves with two minima, rather than one, where the corresponding disturbance profiles are either confined essentially to the inner layer (for the larger wavenumber) or else have thickness comparable to the outer layer (for the smaller wavenumber). A quartic point has been determined which corresponds to when the two minima have merged. These features have been seen in previously published works where the porous medium is stratified naturally by having distinct sublayers with greatly different permeabilities or conductivities. It has also been found that the large-H limit and the small-H limit yields the same critical Rayleigh number, although the wavenumber achieved in the latter limit depends on the value of γ.

Whilst our analysis has been comprehensive, it has nevertheless been confined to standard linear stability theory. It is well-known that the LTNE version of the present configuration is subject to subcritical instability, and that strongly nonlinear convection arises at smaller values of Ra than is given by linear theory. We do not know at this stage whether this property will be altered in at least part of (H, γ)-space, but such a numerical analysis will be substantial and it has been deferred to a later paper.

Acknowledgments The first-named author (PMP) wishes to thank the Commonwealth Scholarship Commission at the Association of Commonwealth Universities, London, UK, for funding a Commonwealth Academic Fellowship at the University of Bath. He also wishes to thank the University of Bath for providing the facilities to enable the research presented in this paper. Finally, he wishes to thank the Management and Principal of JSS College, Dharwad, India, for granting leave to travel to the UK.

References

Banu, N., Rees, D.A.S.: Onset of Darcy-Bénard convection using a thermal non-equilibrium model. Int. J. Heat Mass Transfer **45**, 2221–2228 (2002)

Brevdo, L.: Three dimensional absolute and convective instabilities at the onset of convection in a porous medium with inclined temperature gradient and vertical throughflow. J. Fluid Mech. **641**, 475–487 (2009)

Combarnous, M., Bories, S.: Modelisation de la convection naturelle au sein d'une couche poreuse horizontale l'aide d'un coefficient de transfert solide-fluide. Int. J. Heat Transfer **17**, 505–515 (1974)

Homsy, G.M., Sherwood, A.E.: Convective instabilities in porous media with through flow. A.I.Ch.E. J. **22**, 168–174 (1976)
Jennings, A., McKeown, J.J.: Matrix Computation, 2nd edn, p. 427. Wiley (1992)
Johannsen, K., Oswald, S., Held, R., Kinzeelbach, W.: Numerical simulation of three dimensional saltwater-freshwater fingering instabilities observed in a porous medium. Adv Water Resour **29**, 1690–1704 (2006)
Jones, M.C., Persichetti, J.M.: Convective instability in packed beds with throughflow. A.I.Ch.E. J. **32**, 1555–1557 (1986)
Kuznetsov, A.V., Nield, D.A.: The effects of combined horizontal and vertical heterogeneity on the onset of convection in a porous medium with vertical throughflow. Trans. Porous Media **90**, 465–478 (2011)
Nield, D.A.: Convection in a porous medium with inclined temperature gradient and vertical throughflow. Int. J. Heat Mass Transfer **41**, 241–243 (1998)
Nield, D.A., Bejan, A.: Convect. Porous Media, 3rd edn. Springer, New York (2006)
Pieters, G.J.M., Schuttelaars, H.M.: On the nonlinear dynamics of a saline boundary layer formed by through-flow near the surface of a porous medium. Phys. D **237**, 3075–3088 (2008)
Proctor, M.R.E., Jones, C.A.: The interaction of two spatially resonant patterns in thermal convection. Part 1. Exact 1:2 resonance. J. Fluid Mech. **188**, 301–335 (1988)
Rees, D.A.S.: Vertical free convective boundary-layer flow in a porous medium using a thermal nonequilibrium model: elliptical effects. J. Appl. Math. Phys. (ZAMP) **54**, 437–448 (2003)
Rees, D.A.S.: The onset and nonlinear development of vortex instabilities in a horizontal forced convection boundary layer with uniform surface suction. Trans. Porous Media **77**, 243–265 (2009a)
Rees, D.A.S.: Microscopic modelling of the two-temperature model for conduction in periodic and heterogeneous media: three-dimensional media. In: Proceedings of the 4th International Conference on Applications of Porous Media, Istanbul, Turkey. Paper 15 (2009b)
Rees, D.A.S.: Microscopic modelling of the two-temperature model for conduction in periodic and heterogeneous media. J. Porous Media **13**, 125–143 (2010)
Rees, D.A.S., Pop, I.: Local thermal nonequilibrium in porous medium convection. In: Ingham, D.B., Pop, I. (eds.) Transport Phenomena in Porous Media III, pp. 147–173. Pergamon (2005)
Rees, D.A.S., Riley, D.S.: The three-dimensional stability of finite-amplitude convection in a layered porous medium heated from below. J. Fluid Mech. **211**, 437–461 (1990)
Rees, D.A.S., Storesletten, L.: The linear instability of a thermal boundary layer with suction in an anisotropic porous medium. Fluid Dyn. Res. **30**, 155–168 (2002)
Riahi, D.N.: Nonlinear convection in a porous layer with permeable boundaries. Int. J. Non-Linear Mech. **24**, 459–463 (1989)
Shivakumara, I.S.: Boundary and inertia effects on convection in porous media with throughflow. Acta Mech. **137**, 151–165 (1999)
Shivakumara, I.S., Khalili, A.: On the stability of double diffusive convection in a porous layer with through-flow. Acta Mech. **152**, 165–175 (2001)
Shivakumara, I.S., Sureshkumar, S.: Convective instabilities in a viscoelastic-fluid-saturated porous medium with throughflow. J. Geophys. Eng. **4**, 104–115 (2007)
Spotz, W.F.: High-Order Compact Finite Difference Schemes for Computational Mechanics. PhD thesis, University of Texas at Austin, Austin, TX, U.S.A. (1995)
Sutton, F.M.: Onset of convection in a porous channel with net through flow. Phys. Fluids **13**, 1931–1934 (1970)
van Duijn, C.J., Wooding, R.A., Pieters, G.J.M., van der Ploeg, A.: Stability criteria for the boundary layer formed by throughflow at a horizontal surface of a porous medium. Environmental Mechanics: Water, Mass and Energy Transfer in the Biosphere. Geophys. Monogr. **129**, 155–169 (2002)
Wakao, N., Kaguei, S.: Heat and mass transfer in packed beds. Gordon and Breach (1982)
Wooding, R.A.: Rayleigh instability of a thermal boundary layer flow through a porous medium. J. Fluid Mech. **9**, 183–192 (1960)
Wooding, R.A., Tyler, S.W., White, I., Anderson, P.A.: Convection in ground water below an evaporating salt lake: 1. Onset of instability. Water Resour. Res. **33**, 1199–1217 (1997a)
Wooding, R.A., Tyler, S.W., White, I., Anderson, P.A.: Convection in ground water below an evaporating salt lake: 2. Evolution of fingers or plumes. Water Resour. Res. **33**, 1219–1228 (1997b)